photonics

MDPI

Article

Cost-Effective and Energy-Efficient Photonics-Based Frequency Hopping by Single Wavelength-Tunable Laser for Secure THz Communication

Naoto Masutomi [1,*], Shenghong Ye [1], Bo Li [1], Ryota Kaide [1], Ming Che [1], Yuya Mikami [1], Yuta Ueda [2] and Kazutoshi Kato [1]

[1] Graduate School of Information Science and Electrical Engineering, Kyushu University, Fukuoka 819-0395, Japan; ye.shenghong.983@s.kyushu-u.ac.jp (S.Y.); li.bo.641@s.kyushu-u.ac.jp (B.L.); kaide.ryota.499@s.kyushu-u.ac.jp (R.K.); che.ming.677@m.kyushu-u.ac.jp (M.C.); mikami@ed.kyushu-u.ac.jp (Y.M.); kato@ed.kyushu-u.ac.jp (K.K.)

[2] NTT Device Technology Laboratories, NTT Corporation, Atsugi 243-0198, Japan; yuta.ueda.dh@hco.ntt.co.jp

* Correspondence: masutomi.naoto.153@s.kyushu-u.ac.jp; Tel.: +81-92-802-3753

Abstract: A photomixing-based frequency-hopping spread spectrum (FHSS) system is effective for future secure terahertz (THz) wireless communications. Conventional photomixing systems are typically composed of two lasers, which result in an increased system size and power consumption. To address this issue, we applied our proposed THz wave generation method, using a single wavelength-tunable laser, to the FHSS system. In the experiments, we successfully demonstrated a J-band (220–330 GHz) FHSS system with a frequency-hopped interval of 400 ns.

Keywords: terahertz wave; wavelength-tunable laser; photomixing; frequency-hopping spread spectrum

Received: 10 December 2024
Revised: 10 January 2025
Accepted: 13 January 2025
Published: 16 January 2025

Citation: Masutomi, N.; Ye, S.; Li, B.; Kaide, R.; Che, M.; Mikami, Y.; Ueda, Y.; Kato, K. Cost-Effective and Energy-Efficient Photonics-Based Frequency Hopping by Single Wavelength-Tunable Laser for Secure THz Communication. *Photonics* **2025**, *12*, 76. https://doi.org/10.3390/photonics12010076

1. Introduction

In recent years, mobile data traffic has experienced continuous growth, driven by the widespread adoption of mobile devices and the increasing reliance on fifth-generation (5G) communication technology [1–4]. As the demand for mobile connectivity continues to surge, future wireless networks will need to support even larger data capacities to accommodate a greater volume of users, higher data rates, and a broader range of connected devices. To meet this demand, there has been an increasing interest in leveraging electromagnetic waves within the 100 GHz to 10 THz range, known as terahertz (THz) waves, for wireless communications due to their substantial bandwidth potential [5–15]. The THz band occupies an intermediate range between traditional radio waves and light waves, providing it with a broader bandwidth than radio waves and improved transmission capabilities compared to light waves. Thus, THz waves are regarded as promising candidates for future high-capacity wireless communications.

Information security in wireless communication is critically important due to the inherent openness of the communication medium, which leaves it vulnerable to jammers and eavesdroppers [16]. THz communication links have traditionally been considered highly secure in line-of-sight (LOS) conditions due to their strong directivity. On the other hand, recent studies have revealed that even directional links are susceptible to threats such as interference and eavesdropping [17–19]. Since THz links possess strong directivity, a jammer would need to precisely target the receiver to successfully execute an attack.

However, one of the primary advantages of using THz links is the availability of a wide bandwidth, which allows for high data rates. Consequently, the receiver needs to operate across a broad bandwidth, which could negatively impact link security. This is because a jammer could exploit this wide bandwidth to cause interference. Additionally, while the strong directivity of THz waves makes it challenging for an eavesdropper to place a receiver capable of detecting the signal without interfering with the intended receiver, eavesdropping may still be possible by placing a small passive object within the beam. This object could scatter a portion of the radiation to a receiver positioned elsewhere, thus enabling the interception of the signal even in a highly directional THz beam. Moreover, the rapid advancement in computational power has rendered traditional encryption-based security measures insufficient. In this context, a physical-layer-security (PLS)-based system is effective.

PLS protects information by leveraging the physical characteristics of the communication system and external random noise [20]. A paper [21] has demonstrated that PLS can enhance the confidentiality of wireless communication systems. By using PLS technology, the computational load is reduced compared to traditional encryption methods, and a higher level of confidentiality can be achieved. Additionally, PLS can be combined with existing security mechanisms, contributing to the establishment of highly reliable wireless links. For example, PLS technology using intelligent reflecting surfaces (IRSs) [22–24] has been proposed for secure THz communication; however, it has the drawback of increasing system complexity. In systems that use quantum noise to mask THz signals, the randomness of quantum noise prevents eavesdroppers from detecting the signal [25]. However, challenges related to cost and device complexity remain obstacles for practical implementation. Furthermore, in a wireless transmission system that uses two THz beams and coherent detection, security is enhanced, as the data cannot be recovered, even if one of the beams is intercepted [26]. However, this approach results in a larger transmission system.

In recent years, there has been active research on applying the frequency-hopping spread spectrum (FHSS), widely used in secure microwave communication [27], to the THz band [28]. The FHSS framework is a technique that uses multiple frequency channels as carrier frequencies and transmits data by hopping the carrier frequency between different channels at fixed intervals. Figure 1a,b illustrate the carrier frequency undergoing rapid pseudo-random changes, a fundamental characteristic of the FHSS framework. Even if an unauthorized user attempts to jam the signal during a single hopping interval, they cannot predict the carrier frequency for the next interval. This unpredictability ensures that the signal can resume transmission in subsequent intervals without interruption. As a result, FHSS minimizes the risk of persistent jamming and prevents complete eavesdropping of the transmitted information. However, FHSS demands a wide bandwidth, which aligns well with the bandwidth-abundant THz region. In electronics-based THz technologies, the frequency-hopping range is limited to a few tens of GHz due to the constraints imposed by frequency multipliers [29]. In contrast, photonic-based THz wave generation methods offer a tuning range exceeding 100 GHz, allowing for more carrier frequency channels, and thereby increasing both the complexity and security of FHSS systems. For example, the study in [30] demonstrated FHSS technology in the 110 GHz to 170 GHz frequency range using two distributed feedback (DFB) lasers. Additionally, in our research, we demonstrated an FHSS system in the 300 GHz band using a tunable DFB laser array (TLA) [31]. Furthermore, we demonstrated an FHSS system in the 300 GHz band with a fast channel transition time on the order of nanoseconds, using a frequency-fixed laser and a high-speed wavelength-tunable laser (TL) [32]. However, since these studies use two lasers as light sources, an increase in the number of system components and power consumption is expected due to the need for laser drive circuits and temperature controllers. To address

this issue, we have devised a photonic-based THz wave generation method consisting of a single TL and have demonstrated the feasibility of this system [33].

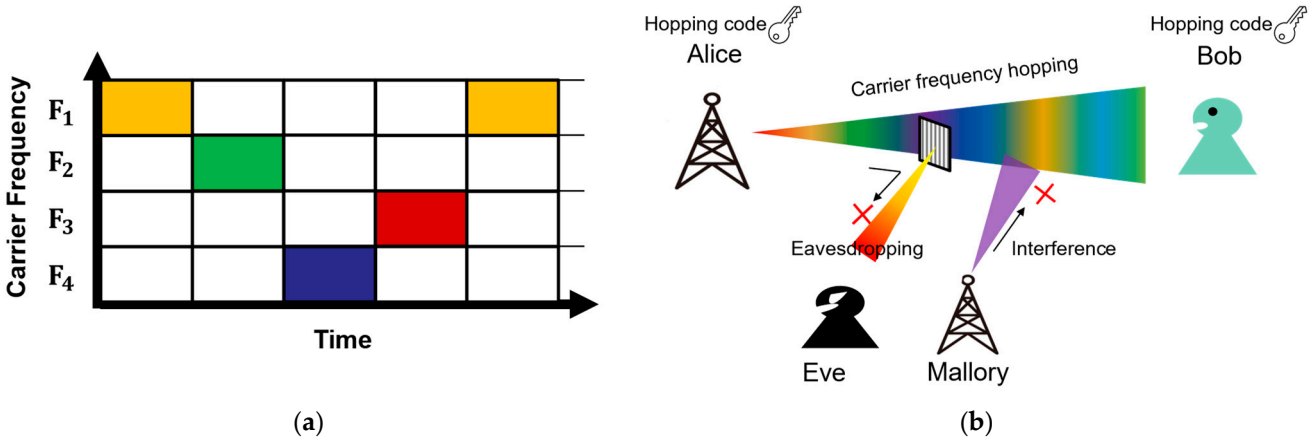

(**a**) (**b**)

Figure 1. (**a**) Carrier frequency hopping at the FHSS and (**b**) conceptual diagram of the FHSS system.

In this study, we developed a cost-effective and energy-efficient photonic-based THz wave generation system for the FHSS that utilizes multiple optical frequencies switched through a single TL. First, the feasibility of switching among multiple optical frequencies using the TL was verified, demonstrating the generation of frequency-hopped THz waves. Next, the proposed method was further validated by successfully generating frequency-hopped THz waves. In this experiment, frequency hopping among three carrier frequencies within the J-band range (220–330 GHz) was achieved with a 400 ns period by switching between four optical frequencies using a single TL.

2. THz Frequency Hopping Using a Single Tunable Laser

In traditional photomixing setups, two lasers are utilized (Figure 2), with the electric fields E_1 and E_2 of their respective light waves expressed as follows:

$$E_1 = A_1 \exp\{j(2\pi f_1 t + \varphi_1)\} \quad (1)$$

$$E_2 = A_2 \exp\{j(2\pi f_2 t + \varphi_2)\} \quad (2)$$

where A_1 and A_2 denote the amplitudes, f_1 and f_2 represent the optical frequencies, and φ_1 and φ_2 are the initial phases. When these light waves are combined and introduced into a uni-traveling-carrier photodiode (UTC-PD), a photocurrent I is produced. This photocurrent is directly proportional to the square of the magnitude of the combined electric fields E_1 and E_2, as expressed in following equation:

$$I \propto |E_1 + E_2|^2 = A_1^2 + A_2^2 + 2A_1A_2\cos\{2\pi(f_1 - f_2)t + (\varphi_1 - \varphi_2)\} \quad (3)$$

A THz wave can be generated by tuning the frequency difference $f_1 - f_2$ to lie within the THz range.

The basic configuration for generating THz waves using a single TL is illustrated in Figure 3a. This setup includes a delayed self-multiplexer along with a laser that alternates between two optical frequencies at intervals corresponding to the THz range, as shown in Figure 3b. The emitted light wave is divided into distinct paths, with one path experiencing a fixed time delay, τ (s). This delay introduces a precise temporal offset between the light waves in the two paths. After the delay, the light waves from both paths are recombined, creating a scenario in which two light waves with distinct frequencies coexist simultaneously, as depicted in Figure 3c. These recombined light waves, now carrying two different

optical frequencies, are subsequently directed into a UTC-PD. Within the UTC-PD, the interaction between the two frequencies generates a THz wave with a frequency f_{THz1}, which corresponds to the difference between the two optical frequencies, as illustrated in Figure 3d. This configuration provides a streamlined and efficient method for THz wave generation, leveraging the frequency-switching capability of a single TL combined with the delayed self-multiplexing technique.

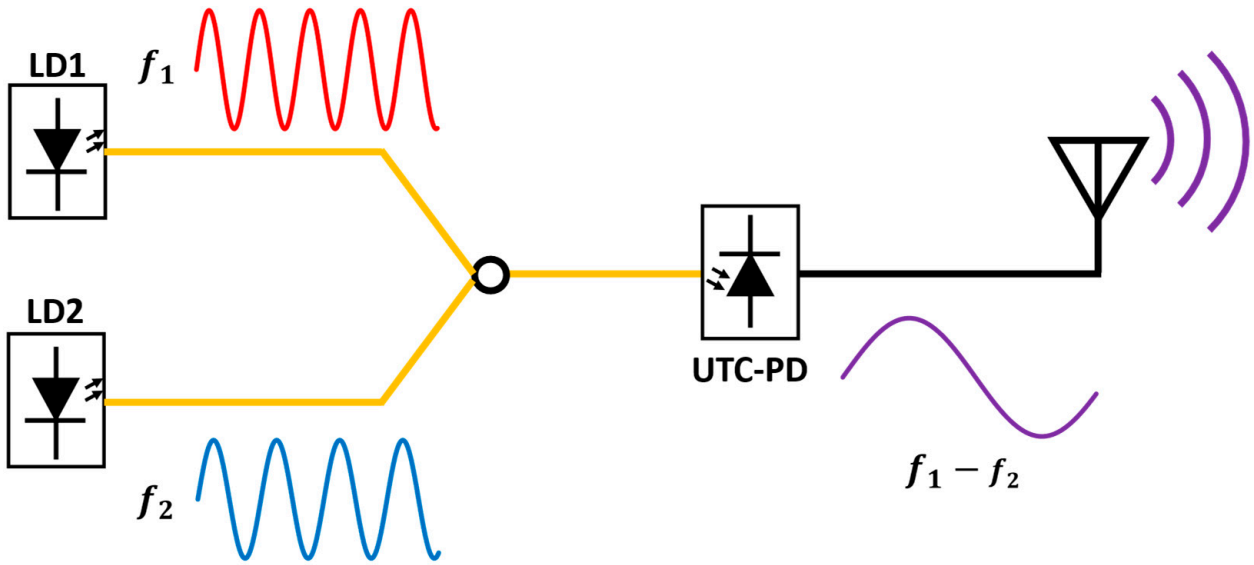

Figure 2. Conceptual diagram of conventional photomixing consisting of two lasers.

This system is applied to construct a new photonic-based FHSS system. For example, the optical frequencies are switched among f_0, f_1, f_2, and f_3, which are related as follows (Figure 3e):

$$f_1 - f_0 = f_{\mathrm{THz1}} \tag{4}$$

$$f_2 - f_0 = f_{\mathrm{THz2}} \tag{5}$$

$$f_3 - f_0 = f_{\mathrm{THz3}} \tag{6}$$

In this configuration, a single base frequency f_0 serves as a reference, with each of the other frequencies, f_1, f_2, and f_3, representing a different offset from this base frequency, thereby generating distinct THz frequencies, f_{THz1}, f_{THz2}, and f_{THz3}. As in previous setups, one of the light wave paths is delayed by τ seconds before being recombined with the other paths, as shown in Figure 3f. When the combined light wave, containing the delayed and non-delayed components, is injected into a UTC-PD, it enables the generation of a THz wave that hops among the frequencies f_{THz1}, f_{THz2}, and f_{THz3}. This frequency hopping occurs with a periodicity of 2τ, as depicted in Figure 3g. In this way, by switching among multiple optical frequencies, the system achieves the generation of frequency-hopped THz waves. This capability allows for a more dynamic and secure communication scheme, as the THz wave can rapidly shift among multiple frequencies, making it highly suitable for applications requiring robust FHSS methods in high-frequency THz bands.

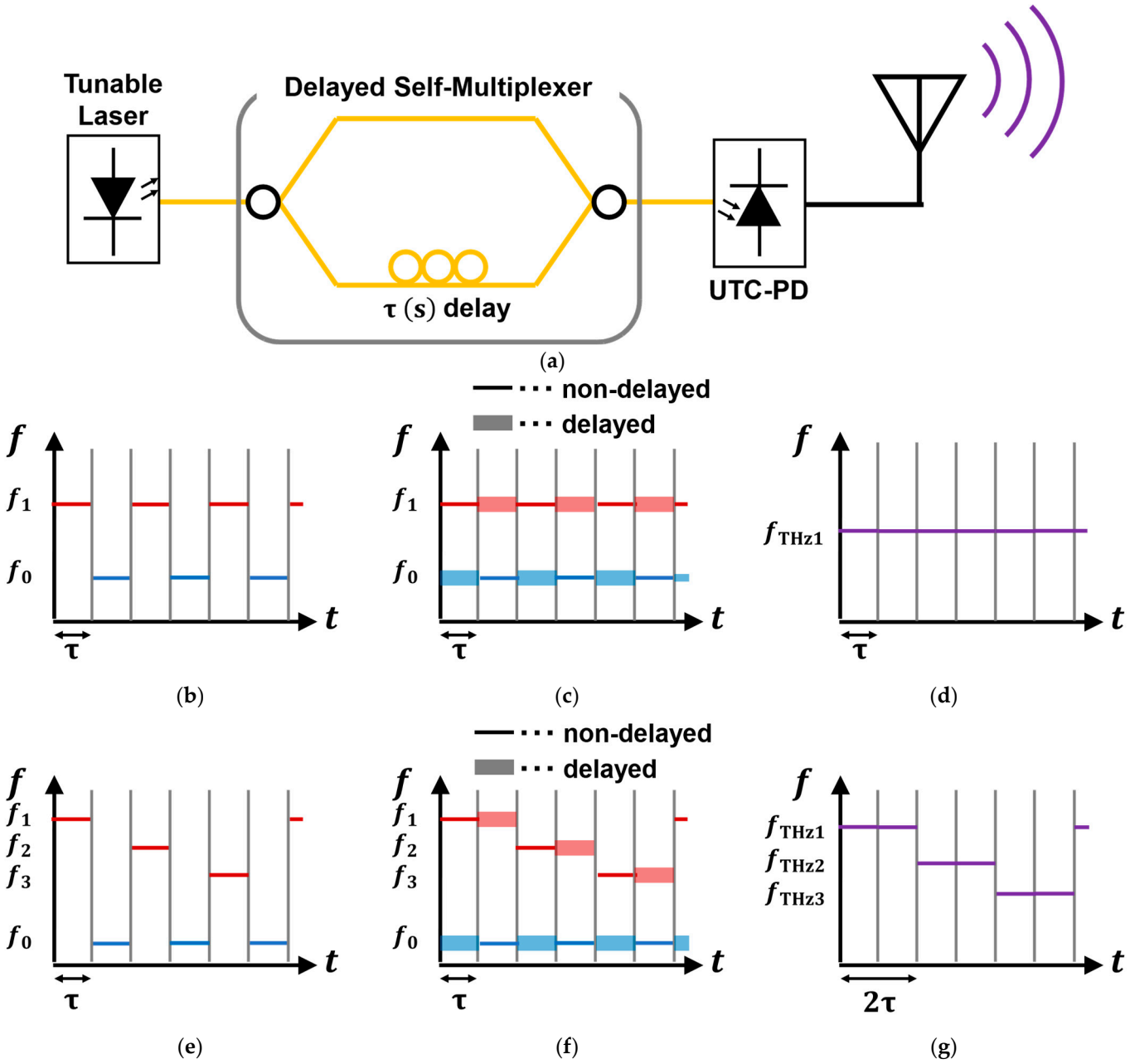

Figure 3. (**a**) Conceptual diagram of photomixing with a single TL; (**b**) Optical frequency from the TL; (**c**) Optical frequency after delayed self-multiplexer; (**d**) THz wave generated by photomixing; (**e**) Optical frequency for generating a frequency-hopped THz wave; (**f**) Optical frequency for frequency-hopped THz wave generation after a delayed self-multiplexer; (**g**) Frequency-hopped THz wave generated by a single TL.

3. Reflection-Type Transversal Filter Laser

The reflection-type transversal filter (RTF) laser used in this study is a TL capable of controlling its optical frequency through the geometric structure of its resonator and the electro-optic (EO) effect [34]. A schematic of the resonator is shown in Figure 4, where the active layer (ACT) and five delay lines are connected by a 1 × 5 multi-mode interference (MMI) coupler. The five delay lines are of different lengths, forming an optical frequency filter. Each delay line and MMI has four wavelength control electrodes, named "Red", "Blue", "Fine", and "Phase". By applying voltage to these electrodes, the refractive index of the delay lines changes due to the EO effect. Consequently, the optical path length changes, altering the filter characteristics and allowing for the selection of the optical frequency. Due

to this structure, the RTF laser achieves 500 ps frequency switching via the EO effect, a tuning range covering the entire C-band from 1530 nm to 1565 nm, power consumption below 10 mW during wavelength switching, and a narrow linewidth of 350 kHz.

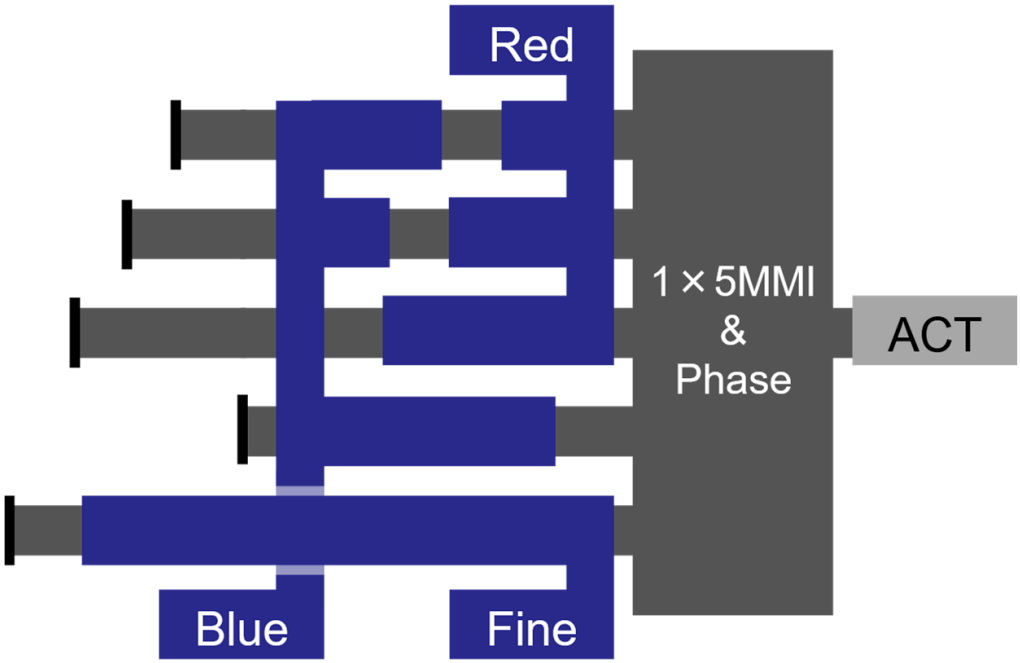

Figure 4. Schematic diagram of the RTF laser's resonator.

Of the four wavelength control electrodes, "Red" and "Blue" have a free spectral range (FSR) of 35 nm, with opposite directions of frequency shift, while "Fine" has an FSR of 1.7 nm, enabling discrete frequency switching. "Phase" allows for finer, continuous changes in the optical frequency. In this study, the "Blue" and "Fine" electrodes are used to switch the optical frequency between four frequencies, as shown in Figure 3e. Figure 5 shows a map of the frequency changes measured when the applied voltages to the Blue and Fine electrodes are varied independently. The applied voltage was changed in increments of 0.5 V, with color differences representing variations in frequency. In this figure, the subtle color changes when varying V_{Fine} indicate frequency changes of approximately 40 GHz, while the more prominent color changes when varying V_{Blue} indicate frequency changes of approximately 300 GHz. To generate THz waves using a single TL, the difference between f_0 and the other frequencies must fall within the THz range, as shown in Equations (4)–(6). In Figure 5, the white point f_0 represents 192.4463 THz, while the black points f_1, f_2, and f_3 represent 192.7663 THz, 192.7256 THz, and 192.6849 THz, respectively. By alternately switching between f_0 and the other frequencies, the proposed method generates THz waves with frequencies of f_{THz1} = 320.0 GHz, f_{THz2} = 279.3 GHz, and f_{THz3} = 238.6 GHz in the experiment using a J-band UTC-PD.

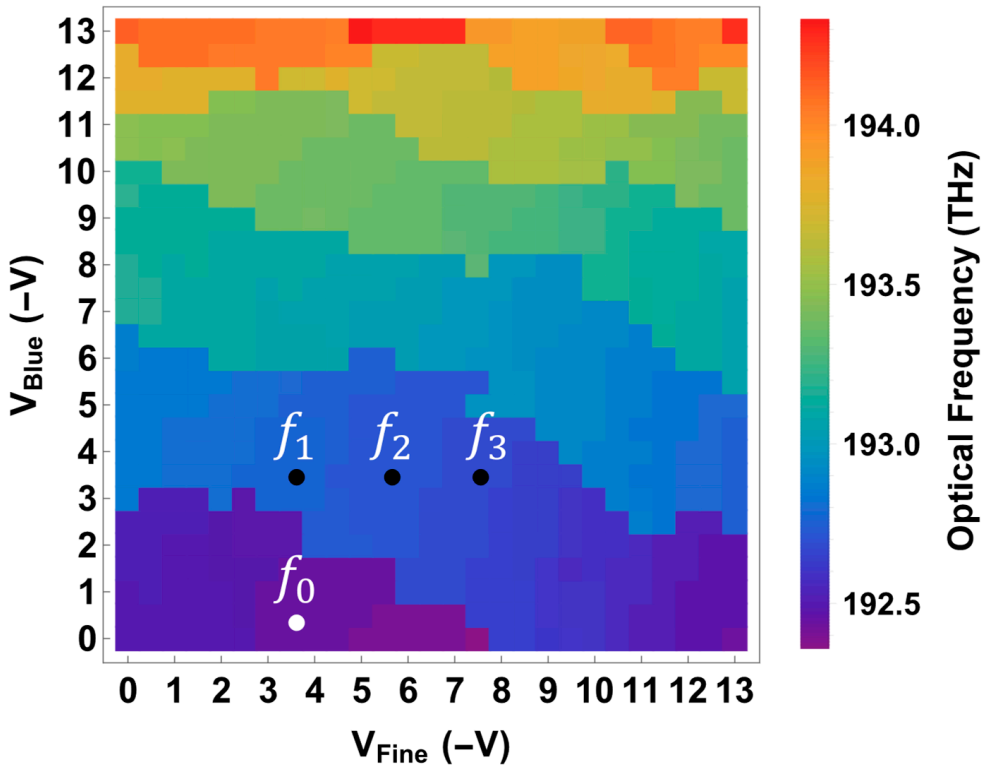

Figure 5. Optical frequency map of the RTF laser when varying V_{Blue} and V_{Fine}.

4. Experiments for Generating Frequency-Hopped THz Wave by a Single TL

4.1. Demonstration of Switching Among Four Frequencies in the RTF Laser

Figure 6 shows the experimental setup for verifying the frequency switching of the RTF laser. First, a voltage pattern with changes every 200 ns was applied to the Blue and Fine electrodes of the RTF laser using a two-channel digital-to-analog converter (DAC). The light wave emitted from the laser was filtered through a tunable optical bandpass filter (TOBF), then introduced into a photodetector (O/E), and the changes in optical intensity over time were recorded on an oscilloscope (OSC). This process was repeated by continuously shifting the center frequency of the TOBF, and the optical intensity was plotted on a frequency–time map. The TOBF's bandwidth was set to 10 GHz, with the center frequency shifted in 5 GHz increments.

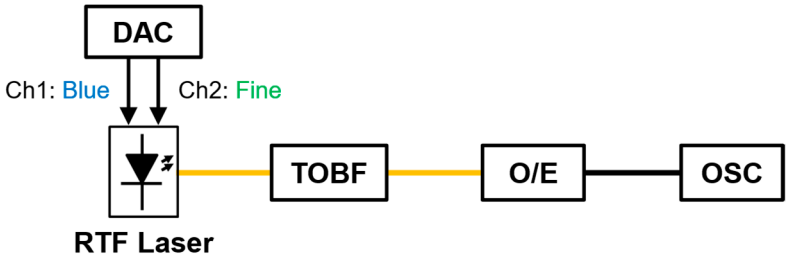

Figure 6. A setup for measuring transitions in the optical frequencies of the RTF laser.

Figure 7a shows the applied voltages to the Blue and Fine electrodes of the RTF laser, respectively, while Figure 7b shows the corresponding changes in the optical frequency of the RTF laser in response to these voltage variations. The peak width does not indicate the linewidth of the light wave, but rather the bandwidth of the TOBF (10 GHz).

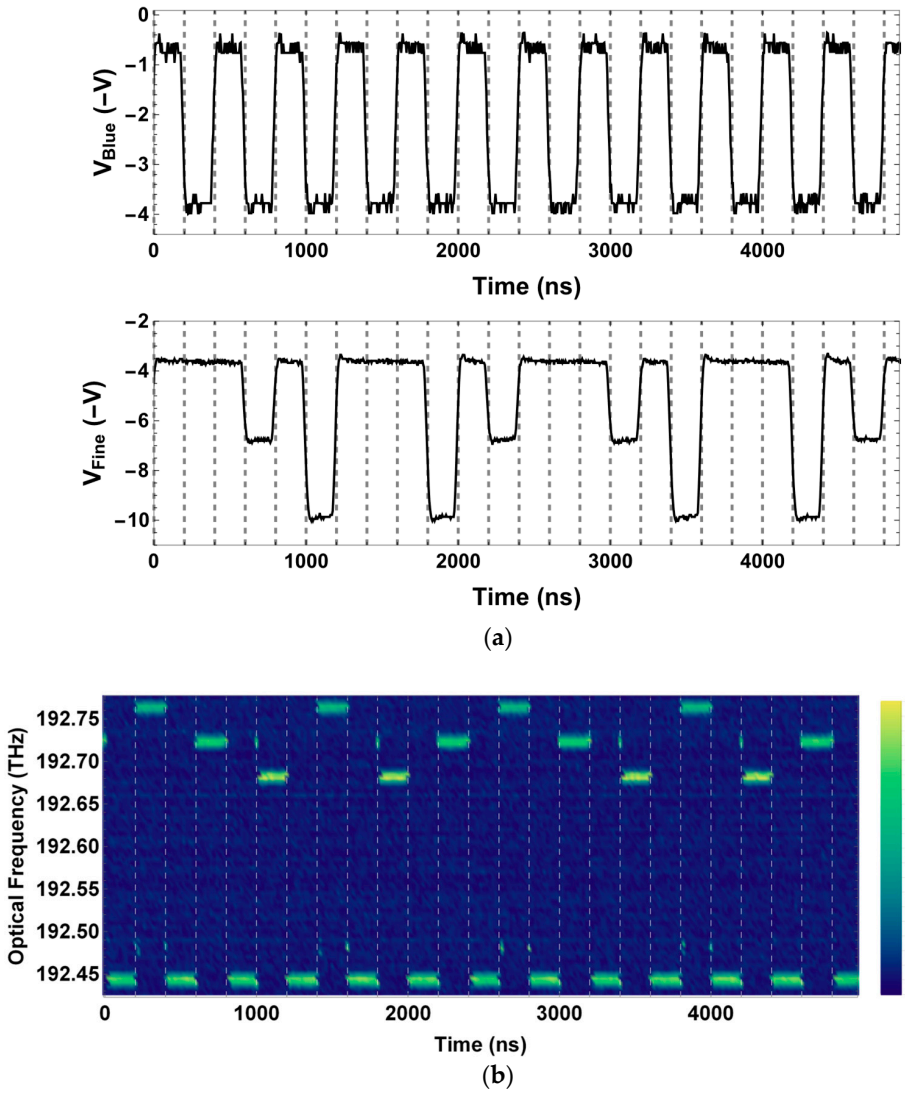

Figure 7. (**a**) Applied voltage to the RTF laser: (**top**) Blue electrode (**bottom**) and Fine electrode; (**b**) Measured optical frequencies of the RTF laser.

From this map, four distinct optical frequencies—192.4463 THz, 192.7663 THz, 192.7256 THz, and 192.6849 THz—were detected. The transitions between these light waves occurred in response to the voltage switching every 200 ns. Thus, the generation of a light wave that alternates among four frequencies at regular intervals was confirmed.

4.2. Demonstration of Frequency Hopping Among Three Frequencies in the 300-GHz Band

The experimental setup for demonstrating frequency hopping within the 300-GHz band using a single RTF laser is illustrated in Figure 8a. Similar to the configuration in the previous section, the RTF laser was applied with the voltage patterns shown in Figure 7a, which were applied to the Blue and Fine electrodes through a two-channel DAC. This configuration enables the RTF laser to switch optical frequencies, as depicted in Figure 7b. Within the delayed self-multiplexer, one of the optical paths is delayed by 200 ns, matching the frequency-switching period of the light waves, before being recombined. Here, after passing through the delayed self-multiplexer, the light waves at four distinct frequencies were continuously observed using an optical spectrum analyzer (OSA), as shown in Figure 8b. Here, the intensity of the light wave with 192.4463 THz is stronger than that of the other light waves because, as shown in Figure 7b, the light wave is output for a longer duration compared to the other frequencies. These light waves were then

directed into the UTC-PD, where THz waves at approximately 238.6 GHz, 279.3 GHz, and 320.0 GHz were expected to be generated. The generated THz waves were subsequently input into a subharmonic mixer (SHM) through a WR-3.4 waveguide for further processing. The frequency of the THz waves generated by the UTC-PD was measured using a down-conversion process. This process involved amplifying the THz signal by mixing it with a local oscillator (LO) signal, which was obtained by multiplying a signal from a signal generator (SG) using a ×12 multiplier. The down-converted signal was then observed on an OSC, enabling the precise frequency measurements of the generated THz waves.

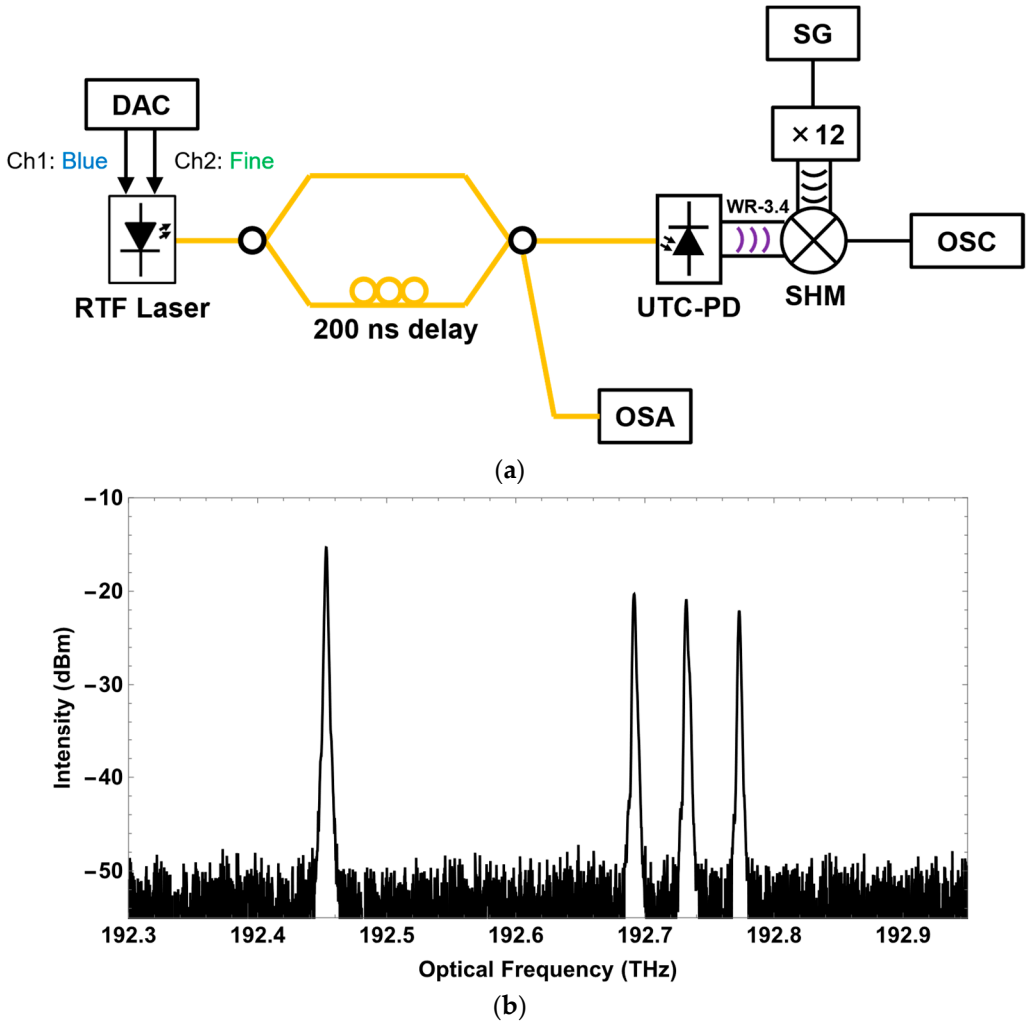

Figure 8. (**a**) Experimental configuration for generating the THz FHSS using a single TL; (**b**) Optical spectrum observed with the OSA.

To configure the LO signal, the SG output frequency was initially set to 10.0 GHz. This frequency was then multiplied by 24 using the ×12 multiplier and the SHM, resulting in an amplified LO signal of 240.0 GHz. With this setup, a THz wave at 238.6 GHz was observed as an intermediate frequency (IF) of 1.4 GHz, as shown in Figure 9a (channel 1). Subsequently, the SG output frequency was adjusted to 11.8 GHz, setting the LO to 283.2 GHz. Under this configuration, the THz wave at 279.3 GHz appeared as an IF of 3.9 GHz, as shown in Figure 9c (channel 2). Further adjustment of the SG output frequency to 13.3 GHz raised the LO to 319.2 GHz, enabling the observation of the THz wave at 320.0 GHz as an IF of 0.8 GHz, as depicted in Figure 9e (channel 3). Figure 9b,d,f illustrate the frequency transitions obtained by analyzing the waveforms observed on the OSC through the short-time Fourier transform (STFT). The STFT analysis provides a time–

frequency representation of the signals, capturing the transitions among the frequencies. Also, when performing a short-time Fourier transform (STFT), the signal was divided into several segments. The parameter nperseg specifies the number of data points within each segment, and, in this analysis, it was set to 256. These results confirm that the system successfully achieved frequency hopping in the J-band frequency range.

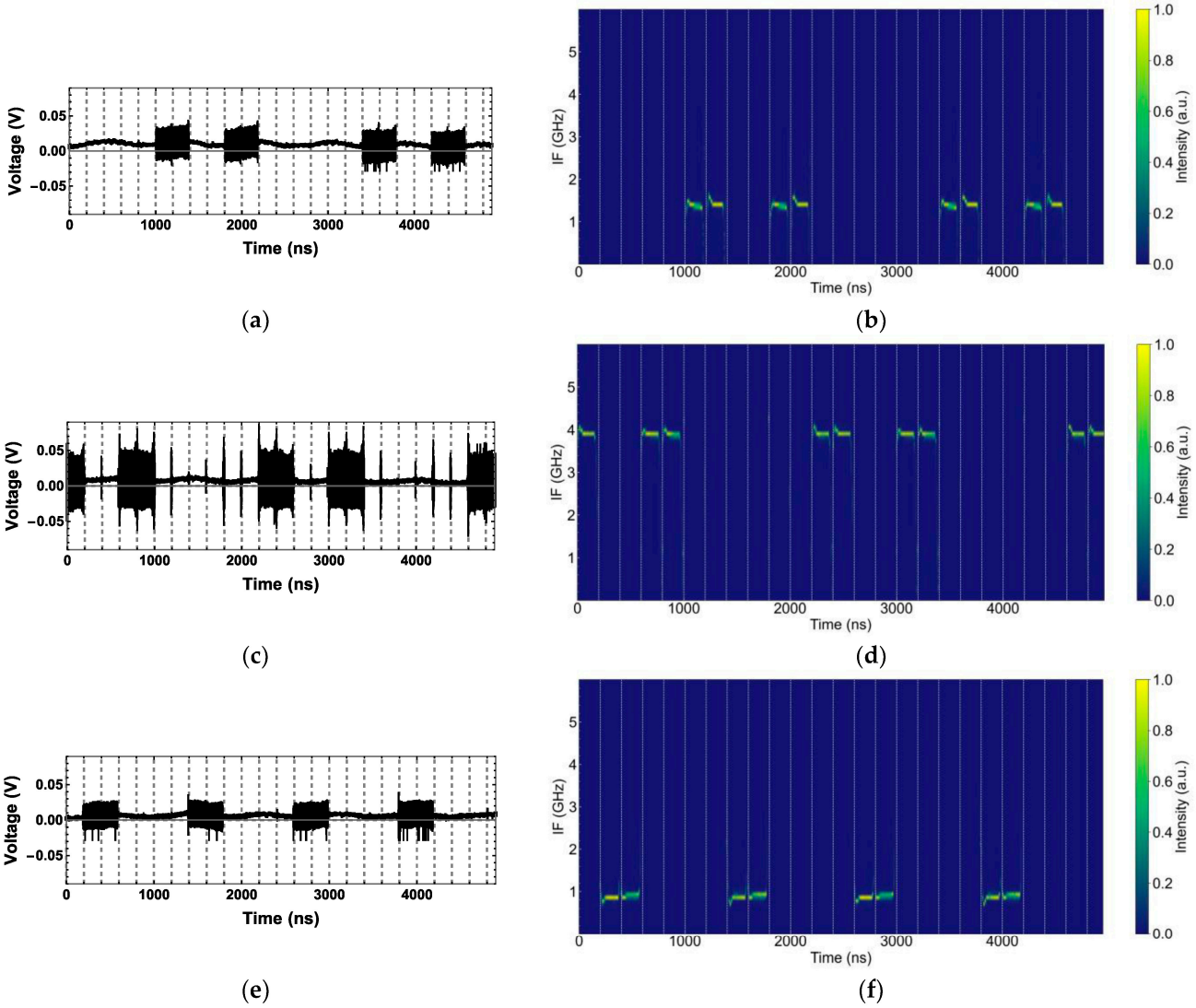

Figure 9. (**a**) The IF signal at the 238.6-GHz wave and 240-GHz LO (channel 1); (**b**) The STFT of channel 1; (**c**) The IF signal at the 279.3-GHz wave and 283.2-GHz LO (channel 2); (**d**) The STFT of channel 2; (**e**) The IF signal at the 320.0-GHz wave and 319.2-GHz LO (channel 3); (**f**) The STFT of channel 3.

5. Discussion

In the FHSS, data transmission cannot occur during channel switching (transition time) because the signal frequency must stabilize before the data can be reliably transmitted. Also, security can be enhanced by not transmitting data during the transition time. A lengthy transition time can negatively impact the communication efficiency. In this experiment, the channel transition time—defined as the time required to settle within ±1 GHz of the target frequency—was measured at approximately 50 ns. This transition time is significantly shorter than the millisecond-level transition times typically observed in conventional photonic-based FHSS systems employing DFB lasers. Additionally, frequency hopping in the GHz range could allow eavesdroppers to extract data during the transition time

by DSP. Therefore, frequency hopping in the tens of GHz range has been demonstrated. Furthermore, a brief period of frequency instability, lasting around 50 ns, occurs at the center of each channel. During this period, data transmission is also restricted. To address this, the receiver can be notified in advance of non-transmission periods, a strategy commonly used in standard FHSS systems to ensure continuous and efficient data transmission. Furthermore, the observed frequency instability is primarily attributed to the frequency switching time of the RTF laser, which is influenced by the voltage switching time of the applied voltage pattern. While the RTF laser itself is capable of switching frequencies within 500 ps, the duration of frequency instability can be further reduced by increasing the steepness of the voltage gradient applied during switching. Optimizing this parameter could shorten the instability period, thereby improving the data transmission efficiency and stability in FHSS applications.

6. Conclusions

In this study, we proposed an FHSS system for secure wireless communication in the 300-GHz band, where THz waves are generated through photomixing using a single TL. We successfully demonstrated the generation of THz waves with frequency hopping, achieving a hopping period of 400 ns and a transition time of just 50 ns. This rapid transition enables highly efficient frequency switching, minimizing non-transmission periods and enhancing the communication stability. With these frequency-hopped THz waves, we verified the feasibility of implementing a photonics-based FHSS system using only a single TL, marking the first demonstration of such a system. This streamlined configuration underscores the potential for compact, secure, and high-speed THz communication systems, advancing the capabilities of photonics-based wireless communication.

Author Contributions: Conceptualization, N.M. and K.K.; methodology, N.M., S.Y., B.L., R.K., M.C., Y.M., Y.U. and K.K.; validation, N.M., S.Y., Y.M. and K.K.; investigation, N.M., S.Y., B.L., Y.M. and K.K.; resources, Y.U. and K.K.; data curation, N.M.; writing—original draft preparation, N.M.; writing—review and editing, Y.M. and K.K.; visualization, N.M.; supervision, Y.M. and K.K.; project administration, K.K.; funding acquisition, Y.M. and K.K. All authors have read and agreed to the published version of the manuscript.

Funding: This work was supported in part by the commissioned research by the National Institute of Information and Communications Technology (NICT), #02801 and #00901, the MIC/SCOPE, #195010002, the MIC/FORWARD, Grant Number: JPMI241010003, and the JSPS KAKENHI, Grant Numbers: JP23K17751 and JP24H00319.

Institutional Review Board Statement: Not applicable.

Informed Consent Statement: Not applicable.

Data Availability Statement: Data available on request.

Conflicts of Interest: Author Yuta Ueda was employed by the company NTT Device Technology Laboratories. The remaining authors declare that the research was conducted in the absence of any commercial or financial relationships that could be construed as a potential conflict of interest.

References

1. Wang, S.; Zhang, X.; Zhang, Y.; Wang, L.; Yang, J.; Wang, W. A Survey on Mobile Edge Networks: Convergence of Computing, Caching and Communications. *IEEE Access* **2017**, *5*, 6757–6779. [CrossRef]
2. Adebusola, J.A.; Ariyo, A.A.; Elisha, O.A.; Olubunmi, A.M.; Julius, O.O. An Overview of 5G Technology. In Proceedings of the 2020 International Conference in Mathematics, Computer Engineering and Computer Science (ICMCECS), Ayobo, Nigeria, 18–21 March 2020. [CrossRef]

3. Ahmed, S.F.; Alam, M.S.B.; Afrin, S.; Rafa, S.J.; Taher, S.B.; Kabir, M.; Muyeen, S.M.; Gandomi, A.H. Toward a Secure 5G-Enabled Internet of Things: A Survey on Requirements, Privacy, Security, Challenges, and Opportunities. *IEEE Access* **2024**, *12*, 13125–13145. [CrossRef]
4. Alhammadi, A.; Al-Alawi, R.M.; Jahdhami, M.A.A.; El-Saleh, A.A.; Ismail, Z.H.; Shamsan, Z.A.; Shayea, I. Revolutionizing Mobile Broadband: Assessing Multicellular Networks in Indoor and Outdoor Environments. *IEEE Access* **2024**, *12*, 120840–120863. [CrossRef]
5. Song, H.J.; Nagatsuma, T. Present and Future of Terahertz Communications. *IEEE Trans. Terahertz Sci. Technol.* **2015**, *1*, 256–263. [CrossRef]
6. Nagatsuma, T.; Horiguchi, S.; Minamikata, Y.; Yoshimizu, Y.; Hisatake, S.; Kuwano, S.; Yoshimoto, N.; Terada, J.; Takahashi, H. Terahertz wireless communications based on photonics technologies. *Opt. Express* **2013**, *21*, 23736–23747. [CrossRef] [PubMed]
7. Nagatsuma, T.; Carpintero, G. Recent Progress and Future Prospect of Photonics-Enabled Terahertz Communications Research. *IEICE Trans. Electron.* **2015**, *E98-C*, 1060–1070. [CrossRef]
8. Akyildiz, I.F.; Han, C.; Hu, Z.; Nie, S.; Jornet, J.M. Terahertz Band Communication: An Old Problem Revisited and Research Directions for the Next Decade. *IEEE Trans. Commun.* **2022**, *70*, 4250–4285. [CrossRef]
9. Seeds, A.J.; Shams, H.; Fice, M.J.; Renaud, C.C. TeraHertz Photonics for Wireless Communications. *J. Light. Technol.* **2015**, *33*, 579–587. [CrossRef]
10. Elayan, H.; Amin, O.; Shihada, B.; Shubair, R.M.; Alouini, M.S. Terahertz Band: The Last Piece of RF Spectrum Puzzle for Communication Systems. *IEEE Open J. Commun. Soc.* **2019**, *1*, 1–32. [CrossRef]
11. Huq, K.M.S.; Busari, S.A.; Rodriguez, J.; Frascolla, V.; Bazzi, W.; Sicker, D.C. Terahertz-Enabled Wireless System for Beyond-5G Ultra-Fast Networks: A Brief Survey. *IEEE Netw.* **2019**, *33*, 89–95. [CrossRef]
12. Yu, X.; Chen, Y.; Galili, M.; Morioka, T.; Jepsen, P.U.; Oxenløwe, L.K. The prospects of ultra-broadband THz wireless communications. In Proceedings of the 2014 16th International Conference on Transparent Optical Networks (ICTON), Graz, Austria, 6–10 July 2014. [CrossRef]
13. Zhang, H.; Zhang, L.; Yu, X. Terahertz band: Lighting up next-generation wireless communications. *China Commun.* **2021**, *18*, 153–174. [CrossRef]
14. Zhang, H.; Yang, Z.; Lyu, Z.; Yang, H.; Zhang, L.; Ozolins, O. 300 GHz photonic-wireless transmission with aggregated 1.034 Tbit/s data rate over 100 m wireless distance. In Proceedings of the 2024 Optical Fiber Communications Conference and Exhibition (OFC), San Diego, CA, USA, 24–28 March 2024. [CrossRef]
15. Maekawa, K.; Yoshioka, T.; Nakashita, T.; Ohara, T.; Nagatsuma, T. Single-carrier 220-Gbit/s sub-THz wireless transmission over 214 m using a photonics-based system. *Opt. Lett.* **2024**, *49*, 4666–4668. [CrossRef]
16. Nguyen, V.L.; Lin, P.C.; Cheng, B.C.; Hwang, R.H.; Lin, Y.D. Security and Privacy for 6G: A Survey on Prospective Technologies and Challenges. *IEEE Commun. Surv. Tutor.* **2021**, *23*, 2384–2428. [CrossRef]
17. Shrestha, R.; Guerboukha, H.; Fang, Z.; Knightly, E.; Mittleman, D.M. Jamming a terahertz wireless link. *Nat. Commun.* **2022**, *13*, 3045. [CrossRef]
18. Ma, J.; Shrestha, R.; Adelberg, J.; Yeh, C.Y.; Hossain, Z.; Knightly, E.; Journet, J.M.; Mittleman, D.M. Security and eavesdropping in terahertz wireless links. *Nature* **2018**, *563*, 89–93. [CrossRef] [PubMed]
19. Li, P.; Wang, J.; Zhao, L.; Gao, X.; Song, F.; Sun, H.; Ma, J. Scattering and Eavesdropping in Terahertz Wireless Link by Wavy Surfaces. *IEEE Trans. Antennas Propag.* **2023**, *71*, 3590–3597. [CrossRef]
20. Mucchi, L.; Jayousi, S.; Caputo, S.; Panayirci, E.; Shahabuddin, S.; Bechtold, J.; Morales, I.; Stoica, R.A.; Abreu, G.; Haas, H. Physical-Layer Security in 6G Networks. *IEEE Open J. Commun. Soc.* **2021**, *2*, 1901–1914. [CrossRef]
21. Wang, N.; Wang, P.; Fanid, A.A.; Jiao, L.; Zeng, K. Physical-Layer Security of 5G Wireless Networks for IoT: Challenges and Opportunities. *IEEE Internet Things J.* **2019**, *6*, 8169–8181. [CrossRef]
22. Chen, W.; Chen, Z.; Ma, X.; Chi, Y.; Li, Z. Secrecy rate optimization for intelligent reflecting surface aided multi-input-single-output terahertz communication. *Microw. Opt. Technol. Lett.* **2020**, *62*, 2760–2765. [CrossRef]
23. Zhu, Y.; Mao, B.; Kato, N. Intelligent Reflecting Surface in 6G Vehicular Communications: A Survey. *IEEE Open J. Veh. Technol.* **2022**, *3*, 266–274. [CrossRef]
24. Qiao, J.; Zhang, C.; Dong, A.; Bian, J.; Alouini, M.S. Securing Intelligent Reflecting Surface Assisted Terahertz Systems. *IEEE Trans. Veh. Technol.* **2022**, *71*, 8519–8533. [CrossRef]
25. Zhang, L.; Deng, Q.; Zhang, H.; Yang, Z.; Pang, X.; Bobrovs, V.; Popov, S.; Wu, Y.; Yu, X.; Ozolins, O.; et al. Quantum Noise Secured Terahertz Communications. *IEEE J. Sel. Top. Quantum Electron.* **2022**, *29*, 8400110. [CrossRef]
26. Kato, K. Photonics-Assisted Terahertz-Wave Beam Steering and Its Application in Secured Wireless Communication. *Photonics* **2022**, *9*, 9. [CrossRef]
27. Liu, Y.; Yang, F.; Yang, Z.; Zhang, L.; Jiang, H.; Chen, F.; Li, M.; Zhang, Z.; Liu, Y.; Zhang, J. Full W-band Photonic Frequency Hopping Generator Based on High-order Optical Frequency Multiplication. In Proceedings of the 2023 International Topical Meeting on Microwave Photonics (MWP), Nanjing, China, 15–18 October 2023. [CrossRef]

28. Yang, Z.; Yang, F.; Wen, Z.; Wang, H.; Liu, Y.; Jiang, H.; Chen, F.; Liu, Y.; Li, M.; Zhang, J. Ultra-Wideband Photonic Frequency-Hopping Waveform Generator Enabled by Optical Injection Locking for Secure Terahertz Wireless Communications. *J. Light. Technol.* **2024**, *42*, 6788–6797. [CrossRef]
29. Li, Z.; Chen, J.; Tang, D.; Zhou, R.; Hong, W. A 205–273-GHz Frequency Multiplier Chain (×6) with 9-dBm Output Power and 1.92% DC-to-RF Efficiency in 0.13-µm SiGe BiCMOS. *IEEE Trans. Microw. Theory Tech.* **2023**, *71*, 2909–2919. [CrossRef]
30. Nallappan, K.; Skorobogatiy, M. Photonics based frequency hopping spread spectrum system for secure terahertz communications. *Opt. Express* **2022**, *30*, 27028–27047. [CrossRef]
31. Li, B.; Ye, S.; Che, M.; Tang, H.; Masutomi, N.; Mikami, Y.; Kato, K. Demonstration of THz Frequency Hopping in the 300 GHz Band Based on UTC-PD and Tunable DFB Laser Array. *Jpn. J. Appl. Phys.* **2024**, *63*, 04SP86. [CrossRef]
32. Ye, S.; Masutomi, N.; Li, B.; Matsumoto, R.; Kaide, R.; Tang, H.; Kamiura, Y.; Che, M.; Mikami, Y.; Ueda, Y.; et al. Photonic Frequency Hopping Driven by High-Speed Wavelength Tunable Laser for Secure Terahertz-wave Communication. In Proceedings of the 2024 Optical Fiber Communications Conference and Exhibition (OFC), San Diego, CA, USA, 24–28 March 2024. [CrossRef]
33. Shiramizu, T.; Seiki, N.; Matsumoto, R.; Masutomi, N.; Mikami, Y.; Ueda, Y.; Kato, K. Feasibility Demonstration of THz Wave Generation/Modulation Based on Photomixing Using a Single Wavelength-Tunable Laser. *Photonics* **2023**, *10*, 369. [CrossRef]
34. Ueda, Y.; Saito, Y.; Shindo, T.; Kanazawa, S.; Kobayashi, W.; Matsuzaki, H.; Ishikawa, M. Hitless Wavelength Switching of Semiconductor Optical Amplifier-Integrated Reflection-Type Transversal Filter Laser with Suppressed Frequency Error. *J. Light. Technol.* **2023**, *41*, 2765–2774. [CrossRef]